Available online at www.sciencedirect.com

ScienceDirect

Procedia Structural Integrity 8 (2018) 126–136

Structural Integrity Procedia

www.elsevier.com/locate/procedia

AIAS 2017 International Conference on Stress Analysis, AIAS 2017, 6-9 September 2017, Pisa, Italy

Study and identification of the thermo-electric behavior of lithium-ion batteries for electric vehicles

Francesco Mocera[a,*], Elena Vergori[a]

[a]*Politecnico di Torino, Corso Duca degli Abruzzi 24, Torino - 10129, Italy*

Abstract

In this paper, the study and the modeling of a lithium-ion battery cell is presented. A programmable electronic load was laboratory designed and realized in order to reduce the cost of the total equipment. The testing system is supplemented with a commercial programmable power supply. This dedicated laboratory equipment can be used to apply cycles according to user defined current profiles. Some tests were performed on the battery cell. The acquired data allowed to carry out the battery modeling and the parameters identification procedure. Finally, the mechanical and the thermal phenomena to which a battery is subjected are presented and discussed.

Peer-review under responsibility of the Scientific Committee of AIAS 2017 International Conference on Stress Analysis

Keywords: lithium-ion battery; battery testing equipment; battery modeling; parameters identification; hybrid vehicles; thermal issues; mechanical failure

1. Introduction

The first Electric Vehicle (EV) was invented in 1834 but then EVs vanished from the scene because of the development of Internal Combustion Engine Vehicles (ICEVs). Nowadays, due to the environmental issue, the interest on EVs and on Hybrid Electric Vehicles (HEVs) is growing again thanks to their lower pollutant emissions. Chan (2002) shows that new studies and technological proposal are continuously involving the automotive field, and

* Corresponding author. Tel.: +39-011-090-6897; fax: +39-011-564-6999.
E-mail address: francesco.mocera@polito.it

Peer-review under responsibility of the Scientific Committee of AIAS 2017 International Conference on Stress Analysis
10.1016/j.prostr.2017.12.014

more recently also the working machinery field as presented by Somà et al. (2016). In the latter, Mocera and Somà (2017) underline that lots of attention has to be put on the architecture design depending on the power requirement of the specific application. The main difference between an ICEV and an EV or HEV is the presence of a battery pack used to power the vehicle. The battery pack is a system of single battery cells connected in series to increase the voltage and in parallel to increase the capacity. Bandhauer et al. (2011) shows that the main limitation to the spread of larger fleets of electric vehicles on the mass market is still related with safety, cost, lifetime and operating temperature ranges performance.

To guarantee the best working conditions, voltage, current and temperature of the single cells are handled by an electronic unit called Battery Management System (BMS) as presented by Barreras et al. (2016).

Traction batteries need characteristics such as high energy density and power density. The Ragone plot represented in Polleta et al. (2012) shows that, among the established technologies, lithium-ion and lithium-polymer cells are the one which best satisfy these requirements. Other advantages addressable to Li-ion batteries are the high cell potential and the high charge/discharge rate as presented by Nitta et al. (2015). However, there are still some drawbacks and they are mainly related with cost, safety, lithium reliability and cycle life. Nevertheless, Conte (2006) says that lithium based cells seem to be the pathway for the HEVs' future.

Further distinction must be introduced within the lithium-ion batteries. A first classification can be done according to the cell's shape and size. A battery cell can be manufactured in different shapes, typically cylindrical, prismatic and pouch. Cylindrical cells have the lowest energy density compared to the others, however they are the cheapest to be produced so they are still widely used also in the automotive field. Prismatic cells have a higher energy density and are characterized by and external hard case. Pouch cells are flexible, can be produced in different formats and are characterized by the higher energy and power density. Since electric vehicles are a focus of interest, the industry trend is toward larger batteries. The design of larger batteries requires to reduce the costs and improve safety, as presented by Bandhauer et al. (2011). In fact, although large cells (prismatic and pouch cell) are lighter and more compact with respect to the energy amount they can store, their cost is higher, the quality of the cells is harder to be guaranteed and the thermal management is a very sensitive aspect because they can store a large amount of energy. On the other hand, smaller cells are favourable for the thermal management and the cost effective. However, in order to obtain the battery pack voltage and capacity needed, many cells must be electrically connected, implying higher chances of failure and energy lost especially due to contact resistance. Therefore, Saw et al. (2014) say that appropriate considerations are required to select the appropriate cell size to build a battery pack for a certain application.

A second classification can be made according to the materials present inside the battery. The main elements inside a battery are the anode, the cathode, the separator between the electrodes and the electrolyte. Nowadays the materials composing the battery electrodes are object of lots of research studies such as Passerini (2016). Most of the research on these batteries has been related to finding the best electrodes material in terms of specific energy, specific power, terminal voltage and cycle life, but with relatively little attention paid to thermal management as underlined by Bandhauer et al. (2011). Nitta et al. (2015) present the typical materials employed for the cell's electrodes. For the anode they are Graphite and more recently Lithium Titanate (LTO). Among the structures used in the cathodes there are Lithium Cobalt Oxide (LCO), Lithium Manganese Oxide (LMO), Nickel Manganese Cobalt Oxide (NMC), Nickel Cobalt Aluminium Oxide (NCA) and Lithium Iron Phosphate (LFP). Conte (2006) points out that there is not a perfect battery with the best performance, but an appropriate compromise must be identified according to the application. Many combinations of anode and cathode materials can be used. Among the commercialized cells, a dominant position is awarded by the LFP-graphite batteries that guarantee the best results in terms of both safety and duration. Bandhauer et al. (2011) says that the cathode material $LiFePO_4$ has been shown to exhibit a superior thermal stability with respect to other chemistries, due to a smaller exothermic heat release.

In the last years, the need to study batteries in real working conditions has increased the demand for high specific testing equipment. With high energy batteries, testing equipment must handle high current rates and the costs connected to these devices are consistent. To contain the costs, some attempts were done to build devices able to discharge batteries like Propp et al. (2015), but always with low current and for low energy batteries. In fact, increasing the current, the heat to be dissipated grows too, and it is necessary to properly dissipate heat in order the system to work in safe operating conditions.

In this paper, the design process of a programmable electronic load is described. Starting from circuits proposed in other studies like that of Jones (2010), we developed our own control circuit on a dedicated printed circuit board. Then the power branch was designed according to the required power target. The programmable electronic load developed, together with a programmable power supply, represents the battery testing system. An appropriate control strategy allows to apply the desiderated current profile to a battery cell. The results obtained with this equipment are presented.

In the following section, the battery model and the parameters identification procedure are carried out. Finally, the mechanical and the thermal phenomena to which a lithium ion battery is subjected are presented and discussed. They can be faced using a mechatronic approach to guarantee safety and provide maintenance of the battery in vehicles application.

2. Programmable test bench

Battery testing systems are becoming more and more important with the renewed interest towards electric vehicles. It is possible to identify two main purposes for such systems: battery modelling and parameters identification with standard current profiles and cell's performance analysis. A battery testing system can be schematically represented as shown in Fig. 1 and it is composed by an electronic load to discharge the battery, a power supply to charge the battery, a computer to give the commands, a Data Acquisition system (DAQ) to acquire data and the battery Cell Under Test (CUT).

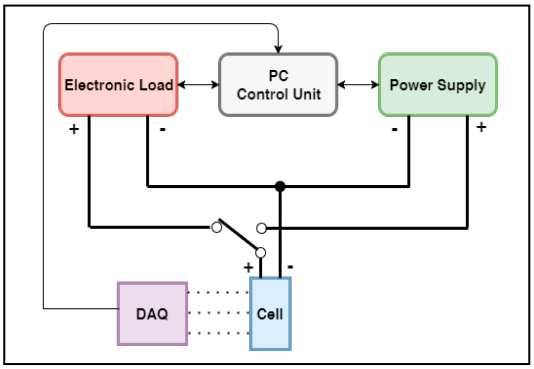

Fig. 1. battery testing system setup.

2.1. The electronic load design

The electronic load is a device that allows to apply a load, which consists in a predefined controlled amount of current to a voltage source that in this application is the battery cell. It is convenient it to be programmable to guarantee the automatization of the test performed. A Programmable Electronic Load (PEL) consists in an array of power MOSFETs used as variable resistors. In fact, a battery cell is not a constant voltage generator and the terminal voltage decreases when the energy stored in the battery is reduced. So, it is necessary a variable resistor to discharge the battery, in order the resulting current profile to be constant and controllable. Thus, a current control loop is required to compensate the battery terminal voltage variations.

In Fig. 2a the schematic of a basic PEL is shown. A voltage reference coming from a filtered PWM_{ref} signal is used to set the predefined current value. This value must be compared with the voltage drop V_1, directly related to the current flowing from the battery. The OP1 applies a higher voltage to the MOSFET gate due to the positive difference between the voltage reference and the feedback reference (non-inverting and inverting port). Thus, increasing the Gate-Source Voltage (V_{GS}) and decreasing the MOSFET Drain-to-Source Resistance (R_{DS}) as direct consequence, the loop allows for current regulation. This basic circuit can be found in most of the PEL available on the market.

(a) (b)

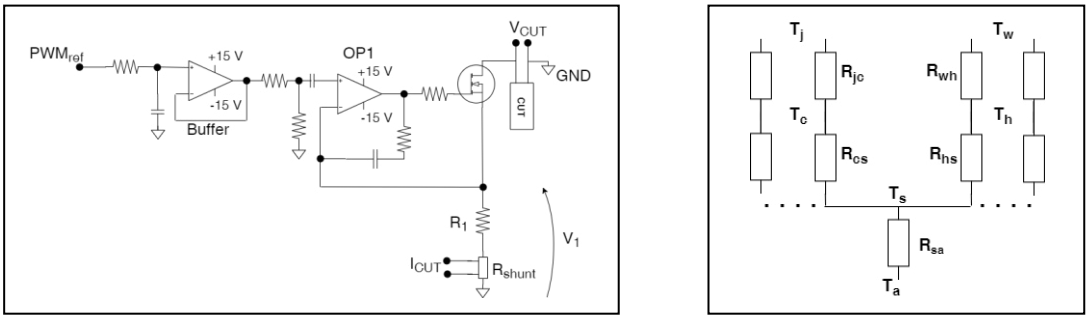

Fig. 2. (a) electronic load control circuit realized on a dedicated printed circuit board, (b) thermo-electric analogy.

The biggest drawback of this architecture is that all the power coming from the battery cell is dissipated as heat within the MOSFETs: the higher the set current, especially in continuous operating mode, the higher is the power dissipation. To prevent the failure of the system, a properly designed cooling system should maintain temperatures in the prescribed value ranges. Looking at commercial solutions, it is usual to find arrays of several MOSFETs connected in parallel to increase the PEL's power dissipation capability. Moreover, distributing the load over several components allows a better heat extraction, optimizing the heat sink surface. Since high temperatures easily bring MOSFETs to failure, the cooling system plays a crucial role in such a device. To design a PEL system, electrical and thermal requirements must be stated:

- Voltage operating range 2.5 – 4 V;
- Maximum current 120 A;
- Maximum continuous power 400 W.

From the first two requirements, the total equivalent resistance R_{eq} of the system can be found. The maximum current must be guaranteed in all the voltage ranges so in the worst case, when the battery is low, $R_{eq} = 0.021\ \Omega$, that can be achieved as a parallel of 4 identical branches of $R_{branch} = 0.084\ \Omega$, each one made by the series of a MOSFET and a resistor. In the present case, a 10 mΩ/50 W power resistor was selected, so the maximum MOSFET resistance should be 74 mΩ. The chosen MOSFET had $R_{DS,on} = 2$ mΩ, with $V_{GS} = 10$ V.

The thermal design of the system can be approached with the thermo-electric analogy, represented in Fig. 2b. In the equivalent electric circuit of a PEL, two main branches can be identified: the FETs' branch and the resistors' one. All the components are physically fixed on the same heat sink. As a first approximation, the same temperature T_S is considered at the interfaces with the heat sink. In Fig. 2b, T_j and T_c are the MOSFET junction and case temperature; R_{jc} and R_{cs} are the MOSFET junction-case and case-sink thermal resistances; T_w and T_h are the resistor internal wire and housing temperature; R_{wh} and R_{hs} are the resistor wire-housing and housing-sink thermal resistances; T_s and T_a are the sink mean temperature and the ambient temperature and R_{sa} is the thermal sink-ambient resistance.

From the thermodynamic, it is possible to compute the thermal resistance between two surfaces knowing their temperatures and the amount of heat involved. Thus, the thermal resistance required to the heat sink can be evaluated with Eq. 1, for both the MOSFET and the resistor.

$$R_{sa} = \frac{(T_{j/w} - T_a) - P_{M/R} * (R_{jc/wh} + R_{cs/hs})}{(P_M + P_R)} \quad (1)$$

where P_M and P_R are the powers dissipated in the MOSFET and in the resistor respectively. The minimum value coming from Eq. 1 will be the more restrictive to be satisfied. Once the equivalent circuit is defined, it is necessary to establish the heat flow within each branch. It is possible to compute the power coming from Joule effect in each branch as the product between the power of the current flowing and the resistance. Neglecting the small resistance

differences between the components in the four branches, the current flowing in each of them is about 30 A. Therefore, the maximum power dissipated in the resistor is about 10 W. The power dissipated in the MOSFET can be evaluated with respect to the maximum power that may involve the branch. Considering the worst condition, when the battery is fully charged, in each branch it is possible to find that P_{branch} is about 120 W. So, P_M is about 110 W. The thermal characteristics of the selected electronic components are the following:

- MOSFET: $R_{jc} = 0.29\ \frac{°C}{W}$, $R_{cs} = 0.24\ \frac{°C}{W}$, $T_{w,max} = 175\ °C$
- Resistor: $R_{wh} = 1.9\ \frac{°C}{W}$, $R_{hs} = 0.06\ \frac{°C}{W}$, $T_{w,max} = 220\ °C$

A conservative approach is followed by assuming a maximum case temperature of about 80 °C for both components. The limitation is imposed on the case temperature because it can be easily measured, and then it is expressed as a limitation on the junction/wire temperature. According to their R_{jc} and R_{wh}, is results respectively in a junction and a wire temperature of about 112 °C and 100 °C that correspond to a percentage of the maximum junction/wire temperature of about 65 % and 45 %. These values are considered sufficiently conservatives so they are used to design the heat sink. Assuming an ambient temperature of 30 °C, from Eq. 1 it results that the more restrictive condition comes from the MOSFET branch and it is R_{sa}=0.2 °C/W, so it becomes the reference for the heat sink selection. There are several products on the market that satisfy the thermal resistance requirement, but the cost increases with its value decreasing. Thus, a combined solution of a heat sink with a proper fan is adopted to reduce the cost of the system.

2.2. The control system of the testing equipment

The PEL allows to discharge a battery cell with predefined current profiles. A proper power supply must be used to supply energy in charging conditions. As shown in Fig. 3a, the two devices are connected in parallel to the CUT so that a proper programming sequence allows to switch from the discharging to the charging phase depending on the specific test cycle. Each device communicates with a personal computer through a serial communication. A specific software written in MATLAB allows to define a predefined current pattern and manages the communication with the devices. Charging and discharging current reference signals are given to the device together with on/off signals for their internal switches. In this way, it is possible to physically disconnect each of them from the CUT. The electronic load resulting from the design process was realized and is shown in Fig. 3b.

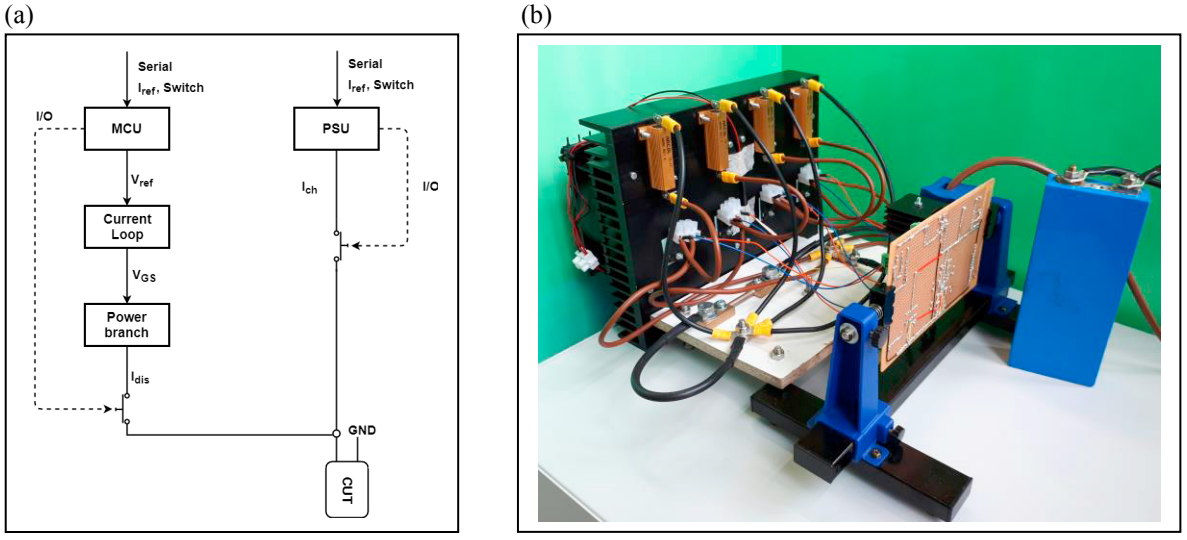

Fig. 3. (a) logic control strategy, (b) electronic load realized.

3. Generated current profiles

In this section, the data acquired with the built equipment are presented. In Figs. 4a and 4b respectively, a Dynamic Stress Test (DST) profile and a Hybrid Pulse Power Characterization (HPPC) test profile are shown. In both cases, the current during the processes of charging and discharging can be suitably controlled.

(a) (b)

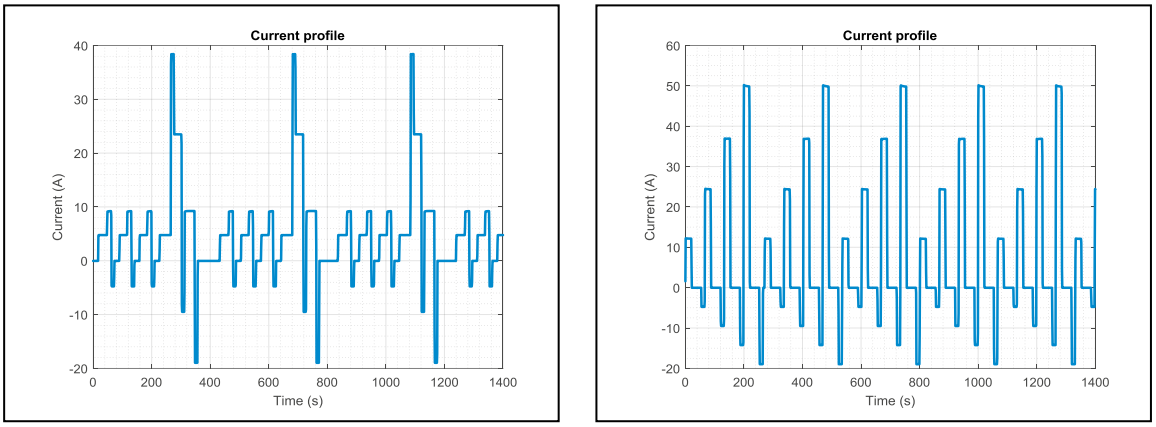

Fig. 4. (a) DST profile, (b) HPPC test profile.

4. Battery modeling

The battery cell under test is a $LiFePO_4$ battery with a nominal capacity of 25 Ah (the key specifications of the battery are summarized in Table 1).

Table 1. $LiFePO_4$ battery cell specifications.

Specifications	
Chemistry	$LiFePO_4$
Nominal Capacity	25 Ah
Nominal Voltage	3.2 V
End-of-charge Voltage	3.65 V
End-of-discharge Voltage	2.0 V
Dimensions (t x w x h)	27 x 70 x 180 mm

The theoretical capacity mainly depends on the quantity of active material that is inside the battery cell. In operating conditions, the capacity of a battery cell is not a constant property, it mainly varies according to the charging/discharging conditions, temperature and ageing. According to the application, the battery can be modelled in different ways. In HEVs and EVs, as a compromise between accuracy and computational effort, the most used models are the equivalent circuit based battery models as summarized by He et al. (2012) and Yang (2016). In literature, such as Hu et al. (2012), many equivalent circuit models exist and can be used according to the degree of detail requested. Some models consider the hysteresis effect observed between the charging and discharging process, others include the self-discharge of the battery.

He et al. (2012) present the most widespread equivalent circuit based battery models that are the Rint model, the Thevenin model with one RC branch and circuits with two or more RC branches.

According to the equivalent circuit based models suggested from the literature, the Rint model was selected because of its simplicity and reduced computational effort. In this model, the battery is represented as a voltage

generator and a series resistor. The voltage generator represents the Open Circuit Voltage (V_{OC}) of the battery, which mainly depends on the State Of Charge (SOC). The V_{OC} is a characteristic of each different battery chemistry. The series resistance represents the internal ohmic resistance of the battery. The Rint model can be expressed by Eq. 2, where V_t is the terminal voltage, I is the current flowing through the battery and R_0 is the ohmic resistance.

$$V_t = V_{OC} - R_0 * I \tag{2}$$

By convention, discharging current is defined positive and charging current is defined negative. In this model, the parameters to be determined are V_{OC} and R_0. Because V_{OC} shows a marked dependency by SOC, in the present paper it is modelled as a function of this quantity according to a simplified electrochemical battery model. In these models, coefficients have no physical meaning and are just used to fit the battery response. Among the simplified electrochemical battery models, the Combined model (Eq. 3) was selected due to the best fitting performance of the battery response.

$$V_{OC} = K_0 - \frac{K_1}{z} - K_2 * z + K_3 * \ln(z) + K_4 * \ln(1 - z) \tag{3}$$

It describes the open circuit voltage as a function of the SOC (indicated by z) using five different coefficients to be able to describe the trend of the whole curve.

5. Battery parameters identification

5.1. Parameters identification procedure

The data acquired with the testing equipment were used to identify the model parameters. The sampling period is very short with respect to the duration of the test so the problem is over-determined. To carry out the model parameters identification, the Least Squares procedure (LS) was adopted. To solve the LS, the QR factorization procedure, explained by Lawson et al. (1974), was implemented due to its good performance also with not well-conditioned coefficients matrices. The identified parameters can be used to reproduce the battery terminal voltage starting from an input current. Among the various discharging profiles generated with the built equipment, the data set obtained with the DST profile was chosen to identify the model parameters. In fact, the DST profile was the one that guaranteed the lowest conditioning number for the coefficients matrix, and so the best regression possible. The dynamic stress test profile was designed by the USABC (US Advanced Battery Consortium) to represent the dynamic EV discharging profile and it consists in a series of positive and negative impulses of different duration. The amplitude and the duration of these impulses is defined by standards in USABC (1996). The total duration of the cycle is 360 seconds. The positive power is the discharging power and the negative one is the charging power. The cycle is iterated in time until the imposed discharging threshold voltage is reached.

The data sets collected during the DST tests were used for the model parameters identification. During the tests, the current and the voltage on the battery terminals were measured. The tests were conducted in air so the main heat transfer mechanism acting was natural convection. The battery was not able to dissipate the whole amount of heat produced so the temperature was growing with current flowing. The external temperature was 27 °C. At first a discharge test with a constant low current was conducted to detect the rated capacity of the battery (capacity test described in PNVG (2001)). Thus, the rated capacity was determined and it was used to compute the state of charge of the battery, according to the Coulomb Counting formulation (Eq. 4).

$$SOC(t) = SOC(0) - \frac{1}{Q_{rated} * 3600} * \int_0^t i(t)\, dt \tag{4}$$

where Q_{rated} is the rated capacity and SOC(0) is the initial state of charge. The SOC during the whole test was computed. The Combined model shows some singularities in SOC=0 and SOC=1, so the corresponding values were not considered. The set of points to be used for the identification process was selected and it was made of time, current, voltage and SOC.

To solve the problem, it is necessary to build the coefficient matrix according to the structure of Eqs. 2 and 3. The coefficients are all the quantities that multiply the parameters K_0, K_1, K_2, K_3, K_4, R_0. The output vector is the output voltage. Starting from these quantities, the triangular orthogonal decomposition was implemented on MATLAB with the function qr. An upper triangular matrix R was obtained, in which the sub-matrices R_k, and y_k can be identified. The unknown parameters can be computed using Eq. 5.

$$\Theta = R_k^{-1} * y_k \tag{5}$$

The parameters obtained can be used to reproduce the battery terminal voltage corresponding to a certain input.

6. Battery issues

Shi et al. (2011) say that studying a battery, three main aspects must be considered to characterize the phenomena occurring in a battery cell, and they are the electrochemical, the thermal and the mechanical phenomena. Many studies have been conducted on the electrochemical aspect, as discussed in the introduction. Relevant studies have been carried out on the thermal aspect too, in particular because of its strong relationship with safety. The research studies in the mechanical field are still in an embryonic phase. In this section, a summary of the most relevant studies to date is presented.

6.1. Mechanical failure

J. M. Hooper and J. Marco (2015) conducted an experimental modal analysis on 25 Ah lithium-ion pouch cells. They found that the natural frequencies of a battery cell are not dependent on the cells state of charge. Some differences can be noted between various cells of the same manufacturer resulting from the manufacturing processes. The first natural frequency of the battery cells occurs at a frequency superior to 180 Hz. Another study conducted by Hooper and Marco (2014) presents the vibration inputs for a series of commercially available EV battery installations. For each vehicle, the vibration energy acting on the battery pack was emulated, considering a representative duration of 100.000 miles. In Europe, they found that most of the road-induced vibration occurs in a frequency range of 0-150 Hz. However, it is important to underline that this vibration energy was measured on the battery pack and not on the single cells, so there may be some differences in the vibration energy experienced by the cells. In fact, Hooper and Marco (2015) underline that higher frequency vibrations may occur because of the presence of the battery management system and the power electronics on the cells, so further research on this subject is needed.

A second research field is that of volumetric changes (swelling) in a single battery cell. Oh et al. (2016) explained that the volume of a lithium-ion cell change mainly because of three reasons in unconstrained conditions and they are the lithium ion intercalation, that is the ability of a positive Li^+ ion to be inserted and extracted from the anode that usually is graphite; the temperature variation and the preload in unconstrained conditions which creates an initial displacement. Regarding intercalation, a mechanical stress is generated in the electrodes during charge and discharge. When the state of charge changes from 0 (full discharge) to 1 (full charge), the thickness of the battery increases by more than 1%. This is mainly because of the anode material that has a larger expansion rate when ions are intercalated compared to that of the cathode material. The stress can cause a fracture of the electrodes over time when cells are cycled.

A third relevant aspect is that related with the mechanical properties of the elements inside a battery cell. During the charging and discharging processes, the separator located between the electrodes is subjected to a certain stress due to the lithium-ion passing across it. Shi et al. (2011) conducted a stress analysis on the separator and showed that the maximum stress is experienced when the battery is fully charged. The anode, the separator and the cathode inside a cell can be wrapped according to different layouts. However, in the resulting structure there always are some areas in which the separator is rounded on the electrodes. The area subjected to the highest stress is that near to the inner corner of the separator in the rounding part. These results were confirmed by impedance testing conducted in Cannarella and Arnold (2013) and Santhanagopalan and Ramadass (2009). Cannarella and Arnold (2013) explained that localized pore-closure of the separator can result in inhomogeneous current distribution which can

result in nonuniform electrode utilization. Finally, thermal effects were demonstrated to be significant in the stress analysis. The simulations revealed that although the thermal expansion increased the average strains in the electrodes and the separator, the local maximum stress and strain in the separator decreased with rising temperature. The maximum Von Mises stress increased with increasing the thickness of the separator and the effective frictions between the separator and its adjacent electrodes. Stress tends to follow the increase of the ion concentration gradient in an electrode. As a result, high C-rates lead to high amplitude of stress. During resting periods, the gradient of the ion concentration gets low, so the stress decreases and vanishes. Stress in the anode is higher than that in the cathode because of different material properties. At a high C-rates, stress might reach its maximum value at the beginning of charge and discharge. The highest stress is generated particularly in the electrode particles near the separator, where cracking and fracture are most likely to take place. The stress-induced diffusion could enhance the ion diffusion in an electrode and reduces the gradient of ion concentration. However, Fu et al. (2013) say that it has little effects on the macro-scale quantities, such as terminal voltage and cell temperature.

6.2. Thermal issues

When current flows within a battery cell, a certain amount of heat is generated. It can be quantified according to Eq. 6 formulated by Bernardi et al. (1985):

$$Q = I * (V_{OC} - V_t) + I * T * \frac{dV_{OC}}{dT} \tag{6}$$

where Q is the heat generation in the battery cell and T is the temperature of the cell. The first term in Eq. 6 is mainly due to ohmic losses in the cell, the second term is the entropic heat.

Measuring the battery surface temperature, the central region of the cell is that in which the highest temperature is reached. However, considering the inner part, the hottest region occurs at the top edge of battery cell while the bottom edge of battery cell has lowest temperature, as presented by Sun et al. (2012). The region close to the positive tab reaches a temperature higher than that at the negative tab. The fully charged cells generate more heat owing to the greater potential difference between the electrodes. Cells of larger capacity drain more current and thus lead to higher heat generation rates as shown by Santhanagopalan and Ramadass (2009). Saw et al. (2014) point out that the heat generated from the cell grows with increasing C-rates. This result is visible in Fig. 5 where the temperature increment during the discharging process is growing quickly with C-rates becoming larger.

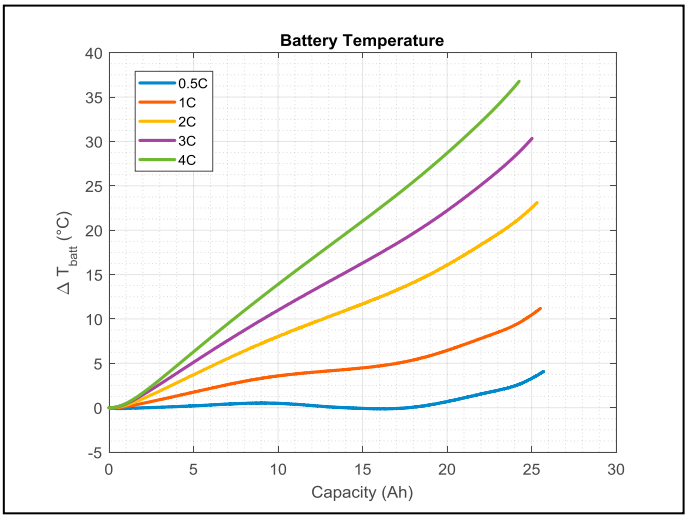

Fig. 5. experimental battery temperature evolution during discharging at various C-rates.

Battery cells are characterized by certain temperature operating ranges and if a battery experiences a temperature outside its safety window, failure events may occur. Joachin et al. (2009) say that safety issues are still the technical barrier for applications such as HEVs, EVs, and PHEVs. The safety of lithium ion batteries, in particular the one associated with thermal runaway hazards, has received lots of attention. Wang et al. (2012) and Lopez et al. (2015) describe thermal runaway as that phenomenon which leads to a chain of exothermic reactions that cannot be stopped which imply excessive heat release, flammable and toxic gas, resulting in fire or explosion. Joachin et al. (2009) say that thermal runaway not only is a safety hazard, but also hinders the performance of lithium-ion batteries. As said before, the major failure mechanism occurring in a battery are mechanical failure, electrochemical failure and thermal failure. All three modes may trigger a severe thermal hazard in a lithium ion battery system. Also internal short circuits can cause severe thermal runaway of lithium ion batteries. Maleki, H. and Howard (2009) conducted a heat transfer analysis in which they shown that less than 1/5 of the total heat released by a battery in a thermal runaway event is enough to trigger the adjacent battery. The presence of fire has little influence on the thermal runaway propagation, however it may cause damage on the accessories located above the battery. The risk of thermal runaway from internal short circuits events can increase with higher cell capacity, especially when the temperature of the internal short circuits and its surroundings exceed the separator melting point and approach the decomposition reaction temperature of cathode material with electrolyte. Santhanagopalan and Ramadass (2009) said that, in almost all scenarios, the origin of the trouble during runaway is from the anode in combination with the electrolyte; so, as a result, a safer design of anodes provides for better chances of surviving an internal short. However, the rapid temperature rise in the cell dominating the overall heat generated during this process, is produced by the cathode reacting with the electrolyte. Therefore, Joachin et al. (2009) underline that it is of utmost importance to find a more structurally stable cathode to use lithium batteries at their fullest potential. During a thermal runaway process, the internal temperature was recorded by Feng et al. (2014) and they found that the temperature difference within the battery was more than 500 °C, while in normal operating conditions it is lower than 1 °C. So, it is meaningful to study the internal temperature for the large format battery.

7. Conclusion

In this work a first approach for testing a lithium-ion battery cell was presented. The design process of a programmable electronic load was performed and the device was realized. This device, coupled with a commercial power supply, was used to charge/discharge a battery cell. The preliminary results obtained with the testing equipment were satisfying. A brief introduction to battery modelling was shown. Among the generated current profile, a DST was performed and the data acquired were used to identify the parameters of the selected battery model. Finally, a focus was conducted on battery's issues as an interesting filed of application under a mechatronic approach to reduce barriers limiting electric vehicles spread. In particular, it was pointed out that to date the major focus is on electrochemical and thermal battery issues, while the study of mechanical failure is still in an embryonic stage so further studies must be conducted on this aspect.

References

Bandhauer, T. M., Garimella, S., Fuller, T. F., 2011, A Critical Review of Thermal Issues in Lithium-Ion Batteries, Journal of the Electrochemical Society, 158 (3), R1-R25.

Barreras, J. V., Fleischer, C., Christensen A. E., Swierczynski, M., Schaltz, E., Andreasen, S. J., Sauer, D. U., 2016, Advanced HIL Simulation Battery Model for Battery Management System Testing, IEEE Transactions on Industry Applications, 52 (6), 5086-5099.

Bernardi, D., Pawlikowski, E., Newman, J., 1985, A general energy balance for battery systems, Journal of the Electrochemical Society, 132 (1), 5-12.

Cannarella J., Arnold, C. B., 2013, Ion transport restriction in mechanically strained separator membranes, Journal of Power Sources, 226, 149-155.

Chan, C. C., 2002, The State of the Art of Electric and Hybrid Vehicles, Proceedings of the IEEE, 90 (2), 247-275.

Conte, F. V., 2006, Battery and battery management for hybrid electric vehicles: a review, Elektrotechnik und Informationstechnik, 123 (10), 424-431.

Feng, X., Fang, M., He, X., Ouyang, M., Lu, L., Wang, H., Zhang, M., 2014, Thermal runaway features of large format prismatic lithium ion battery using extended volume accelerating rate calorimetry, Journal of Power Sources, 255, 294-301.

Fu, R., Xiao, M., Choe, S. Y., 2013, Modeling, validation and analysis of mechanical stress generation and dimension changes of a pouch type high power Li-ion battery, Journal of Power Sources, 224, 211-224.

He, H., Xiong, R., Guo, H., Li, S., 2012, Comparison study on the battery models used for the energy management of batteries in electric vehicles, Energy Conversion and Management, 64, 113–121.

Hooper, J. M., Marco, J., 2014, Characterizing the in-vehicle vibration inputs to the high voltage battery of an electric vehicle, Journal of Power Sources, 245, 510-519.

Hooper, J. M., Marco, J., 2015, Experimental modal analysis of lithium-ion pouch cells, Journal of Power Sources, 285, 247-259.

Hu, X., Li, S., Peng, H., 2012, A comparative study of equivalent circuit models for Li-ion batteries, Journal of Power Sources, 198, 359-367.

Joachin, H., Kaun, T. D., Zaghib, K., Prakash, J., 2009, Electrochemical and Thermal Studies of Carbon-Coated LiFePO4 Cathode, Journal of the Electrochemical Society, 156 (6), A401-A406.

Jones, D., 2010, # EEVblog #102 - DIY Constant Current Dummy Load for Power Supply and Battery Testing, http://youtu.be/8xX2SVcItOA.

Lawson, C. L., Hanson, R. J., 1974, Solving least squares problems, Prentice-Hall Inc., Englewood Cliffs, N.J..

Lopez, C. F., Jeevarajan J. A., Mukherjee, P. P., 2015, Experimental Analysis of Thermal Runaway and Propagation in Lithium-Ion Battery Modules, Journal of the Electrochemical Society, 162 (9), A1905-A1915.

Maleki, H., Howard, J. N., 2009, Internal short circuit in Li-ion cells, Journal of Power Sources, 191 (2), 568-574.

Mocera, F., Somà, A., 2017, Study of a Hardware-In-the-Loop bench for hybrid electric working vehicles simulation, Ecological Vehicles and Renewable Energies (EVER).

Nitta, N., Wu, F., Lee J. T., Yushin, G., 2015, Li-ion battery materials: present and future, Materials Today, 18 (5), 252-264.

Oh, K. Y., Samad, N. A., Kim, Y., Siegel, J. B., Stefanopoulou A. G., Epureanu, B. I., 2016, Novel phenomenological multi-physics model of Li-ion battery cells, Journal of Power Sources, 326, 447–458.

Passerini, S., Scrosati, B., 2016, Lithium and Lithium-Ion Batteries: Challenges and Prospects, The Electrochemical Society Interface, 25 (3), 85-87.

PNGV Battery Test Manual Revision 3, 2001, DOE/ID-10597.

Polleta, B. G., Staffellband I., Shang, J. L., 2012, Current status of hybrid, battery and fuel cell electric vehicles: From electrochemistry to market prospects, Electrochimica Acta, 84, 235–249.

Propp K., Fotouhi A., Auger, D. J., 2015, Low-Cost Programmable Battery Dischargers and Application in Battery Model Identification, Computer Science and Electronic Engineering Conference (CEEC), 225-230.

Santhanagopalan, S., Ramadass, P., 2009, Analysis of internal short-circuit in a lithium ion cell, Journal of Power Sources, 194 (1), 550-557.

Saw, L. H., Somasundaram K., Ye Y., Tay, A. A. O., 2014, Electro-thermal analysis of Lithium Iron Phosphate battery for electric vehicles, Journal of Power Sources, 249, 231-238.

Shi, D., Xiao, X., Huang, X., Kia, H., 2011, Modeling stresses in the separator of a pouch lithium-ion cell, Journal of Power Sources, 196 (19), 8129-8139.

Somà, A., Bruzzese, F., Mocera, F., Viglietti, E., 2016, Hybridization factor and performance of hybrid electric telehandler vehicle, IEEE Transactions on Industry Applications, 52 (6), 5130-5138.

Sun, H., Wang, X., Tossan, B., Dixon, R., 2012, Three-dimensional thermal modeling of a lithium-ion battery pack, Journal of Power Sources, 206, 349-356.

USABC, Electric Vehicle Battery Test Procedures Manual Revision 2, 1996, DOE/ID-10479, http://www.uscar.org/guest/article_view.php?articles_id=74.

Wang, Q. S., Ping, P., Zhao, X. J., Chu, G. Q., Sun, J. H., Chen, C. H., 2012, Thermal runaway caused fire and explosion of lithium ion battery, Journal of Power Sources, 208, 210-224.

Yang, F., Xing, Y., Wang, D., Tsui, K. L., 2016, A comparative study of three model-based algorithms for estimating state-of-charge of lithium-ion batteries under a new combined dynamic loading profile, Applied Energy, 164, 387–399.